AIAA JOURNAL
Vol. 47, No. 6, June 2009

Enhanced 2-D Modeling Technique for Single-Sided Patch Repairs

Marco Boscolo,* Giuliano Allegri,† and Xiang Zhang‡
Cranfield University, Bedfordshire, England MK43 0AL, United Kingdom

DOI: 10.2514/1.42184

This paper reviews the current modeling techniques in the literature and proposes a new one to model bonded patch repaired metallic plates by including all known effects on fatigue crack growth rate. The modeling technique makes use of 2-D plate finite elements and takes into account adhesive progressive failure and the secondary bending effect due to the unsymmetrical configuration of single-sided repair patches. First, comparisons between this 2-D model and a 3-D model were carried out to validate the 2-D bending analysis and the calculated crack-tip stress intensity factors. This modeling technique was then implemented into a computer code interfacing with the commercial finite elements package MSC NASTRAN. Calculated crack growth lives were validated by published experimental tests for three different aluminum plates. Second, the computer code was used to conduct a parametric study on the patch geometries for two different substrate thicknesses showing that for a thinner substrate fatigue crack growth life can be improved by a smaller patch. Finally, a design tool has been developed to determine the most effective patch dimensions for a prescribed fatigue life target.

I. Introduction

METALLIC aircraft structures are subjected to fatigue cracking under service loads. Replacing damaged components is often very expensive; therefore various repair techniques have been developed. Traditional repair methods involve the use of riveted or bolted patches. These methods can be inefficient as fastener holes introduce further stress concentration in the structure. In the last 20 years a repair technique using bonded fiber composite patches has been developed and employed for metallic aircraft components [1]. These patches have been used on the upper and lower wing skins, landing gears, fuselage, and fin skins of the Hercules, Mirage III, and F111 [2].

Although double-sided symmetric repair is more effective, often single-sided patches are applied to damaged (cracked) structures to accommodate the design requirements, for example, maintaining the aerodynamic shape. Consequently, secondary bending is generated by the asymmetric geometry, which reduces the effectiveness of repair due to a higher stress intensity factor (SIF) on the unpatched side of the plate [3]. This results in a faster crack growth rate on the unpatched side and nonuniform crack front profile through the thickness direction. The early analytical method developed by Rose [4] for calculating the limiting value of SIF is not suitable to single-sided repairs because it cannot cope with the secondary bending effect. Young and Sun [5] later developed a method to model the bending effect on SIF using 2-D plate finite elements (FE). Arendt and Sun applied this method to a patch repaired plate and found that not all configurations have a limiting value of SIF [6]. Using 2-D finite elements in conjunction with the modified virtual crack closure technique (MVCCT) [7–9], Sun et al. [10] found a linear distribution of SIF through the thickness of the plate. Wang and Rose [3,11] have claimed that only the rms value of the SIF distribution along the crack front can be calculated by the strain energy based method. However, because the maximum SIF is attained at the unpatched side and needs to be determined, they assumed that the ratio of the maximum SIF to the minimum SIF (at the patched side) was a constant with the crack length and linear function with the maximum and minimum applied stresses. Therefore, a relation between the maximum and rms SIF was found [3].

Single-sided patched plates show a curved crack front under fatigue propagation. One major obstacle in predicting fatigue crack growth (FCG) life for a curved crack front by using a Paris law-type equation is the fact that SIF varies along the crack front, from the patched side to the unreinforced one; there is no single SIF value to describe the crack front stress behavior. Therefore, a representative SIF value is needed for FCG life prediction. The maximum SIF will result in an overconservative prediction because it misses an important range of the SIF values for all other points along the crack front. It is only by averaging the SIF of all points that the error may be maintained at a small level. The mean and the rms values are both good candidates. The latter is related to the total average strain energy release rate [3]. Klug et al. [12] showed that the best agreement with test results, in terms of FCG life, was obtained by using the rms value of SIF distribution.

Recently, 3-D finite element models have been developed to study fatigue crack growth behavior of patch repaired plates taking into account the nonstraight crack front due to asymmetric geometry and secondary bending, for example, [13–16]. These models contain a set of points along the crack front, which are used to calculate the SIF at these points that are then used to estimate the crack growth increment at each point using a material crack growth law that is similar to the Paris law; the crack front is then updated by remeshing the region and running subsequent modeling analyses. Their numerical results were in good agreement with the experiments, even though the disbond between the plate and patch was not considered. In fact, disbond develops during fatigue loading due to stresses being transferred from the cracked plate to the repair patch through the adhesive layer by shear stresses. These shear stresses, if they exceed the adhesive shear strength, will cause adhesive failure and reduction of the effectiveness of the patch repair [12].

The aim of the work presented in this paper was to develop and validate a 2-D modeling technique to calculate the stress intensity factors of single-sided patched plates and use the SIF to predict the crack growth life. The model is much less demanding on computing time and considers all known effects: crack bridging, secondary bending, and adhesive disbond. The main contributions to the field

Presented as Paper 2091 at the 49th AIAA/ASME/ASCE/AHS/ASC Structures, Structural Dynamics, and Materials Conference, Schaumburg, IL, 7–10 April 2008; received 13 November 2008; accepted for publication 8 January 2009.

*Ph.D. Student, Aerospace Engineering Department; m.boscolo@cranfield.co.uk. Member AIAA.

†Lecturer, currently at Bristol University (UK); guiliano.allegri@bristol.ac.uk. Member AIAA.

‡Reader, Aerospace Engineering Department; xiang.zhang@cranfield.co.uk. Member AIAA.

are as follows. First, a novel method to calculate the SIF along the crack front is developed for 2-D plate elements, which leads to a parabolic distribution of the strain energy release rate and an SIF distribution that is the square root of the parabola. Results obtained by this 2-D model are compared with 3-D model results (Sec. IV.B), and a geometrically nonlinear effect is demonstrated (Sec. IV.C). Second, progressive disbond growth is modeled according to a modified Griffith's fracture criterion for mixed failure mode, which interacts with the substrate crack growth; this is different from the main literature, where disbond, if considered, is imposed by experimentally observed shape and size. Third, a weight function is proposed to describe the SIF distribution through the thickness and compute an equivalent SIF value for crack growth life prediction. Comparisons with experiments (from [13]) are made (Sec. IV.D). Finally a parametric study is performed for different patch geometries and a tool to determine the best patch dimension for a given fatigue life target is developed (Sec. IV.E). It is worth mentioning that this modeling technique can be applied also to the design of selective reinforcement using bonded straps [17–19], because the involved failure mechanisms and modeling approach are the same.

II. 2-D Finite Element Model

The mechanisms that need to be modeled for a patched plate are summarized as follows: 1) the stiffening and bridging action done by the patch to a cracked substrate. Part of the substrate stresses is transferred to the patch, which reduces the crack opening stress and crack propagation rate; moreover, the patch also decreases the crack opening displacement by exerting traction (bridging) forces on the crack surfaces. 2) Adhesive progressive failure (disbond) due to the shear stress transfer from substrate to patch. This disbond failure will reduce the stress transfer capability, hence the bridging and stiffening effect. 3) Secondary bending due to unsymmetrical configuration (one-sided patch). This causes higher stresses at the unpatched side of the substrate and lower stress at the patched side producing different crack growth rates along the thickness direction and resulting in a curved crack front. Each mechanism should be modeled to calculate the stress intensity factors for predicting FCG life.

Obviously these 3-D effects can be dealt with by 3-D FE models. Excessive computing power and time will be needed, because a very fine mesh is necessary to avoid the element aspect ratio problem due to the very thin adhesive layer. On the other hand, 2-D models may be used for this problem, but some formulas and techniques must be implemented to correctly model the 3-D effects, that is, displacement variation and continuity in the thickness direction, secondary bending, and crack bridging effect. For this reason, an enhanced 2-D modeling technique that is able to cope with each of the aforementioned effects has been developed.

2-D plate finite elements are employed for the substrate and 2-D laminate or plate elements for the repair patch. Adhesive is modeled by three coincident spring elements to simulate the peel and two transverse shear actions; these springs are connected to two rigid elements to model the adhesive layer thickness (Fig. 1). This adhesive model was originally developed by Tahmasebi [20] for analyzing bonded joints. It is employed in this work to model the progressive cohesive failure of the adhesive by simply deleting the spring elements when disbond occurs. The stiffness values of the spring elements (K_{az} for the peeling action, K_{ax} and K_{ay} for transverse shear) are determined by the following equations:

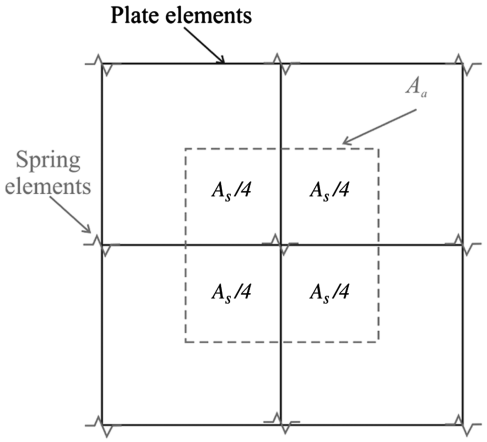

Fig. 2 Area A_a used for calculating the stiffness values of the spring elements to model the adhesive.

$$K_{az} = \frac{A_a E_a}{t_a}, \qquad K_{ax} = K_{ay} = \frac{A_a G_a}{t_a} \tag{1}$$

where A_a is the area of the adhesive element (Fig. 2), E_a is the adhesive elastic modulus, G_a is the adhesive shear modulus, and t_a is the adhesive thickness.

In the model the bottom face of the adhesive is connected to the top of the substrate by means of multipoint constraint (MPC) equations and the Mindlin plate theory [21]. The same is employed for the adhesive/patch interface. Based on the Mindlin theory, with the origin and the x and y axes of the coordinate system on the midplane of the 2-D plate element and the z axis normal to it, the ith-nodal displacement components of a plate element can be written as

$$u(z)_i = u_i^o + z\phi_i^y, \qquad v(z)_i = v_i^o - z\phi_i^x, \qquad w(z)_i = w_i^o \qquad \left(-\frac{t}{2} \le z \le \frac{t}{2}\right) \tag{2}$$

where t is the thickness of the plate element, u_i^o, v_i^o, and w_i^o are, respectively, the nodal membrane displacements in the x, y, and z directions, ϕ_i^y is the nodal rotation around the y axis, and ϕ_i^x is the nodal rotation around the x axis. Naming the nodes that belong to the substrate and connected to the adhesive as nodes s, the nodes that belong to the bottom and top of the adhesive as nodes $a1$ and $a2$, respectively, and the nodes that belong to the reinforcement patch as nodes r (see Fig. 1), the MPC equations can be written as

$$\begin{aligned} u_{a1}^o &= u_s^o + \frac{t_s}{2}\phi_s^y, \qquad v_{a1}^o = v_s^o - \frac{t_s}{2}\phi_s^x, \qquad w_{a1}^o = w_s^o \\ u_{a2}^o &= u_r^o - \frac{t_r}{2}\phi_r^y, \qquad v_{a2}^o = v_r^o + \frac{t_r}{2}\phi_r^x, \qquad w_{a2}^o = w_r^o \end{aligned} \tag{3}$$

where subscripts s, $a1$, $a2$, and r indicate the plane that the nodes belong to (see Fig. 1), and t_s and t_r are the thickness of substrate and reinforcement patch, respectively.

In this way, the 3-D effects and secondary bending are taken into account. The bridging action and adhesive disbond failure are subsequently modeled by this 2-D model as presented in Sec. III.B. Secondary bending is an intrinsic characteristic of one-sided bonded structures; hence a geometric nonlinear analysis is required. Errors

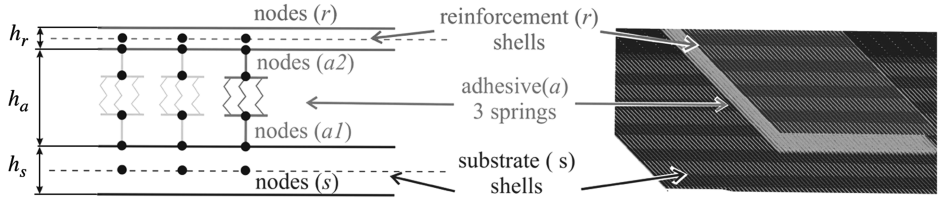

Fig. 1 Schematic of the employed finite elements for modeling the substrate plate, repair patch, and adhesive. Spring nodes are coincident in the model, but are presented as detached for clarity.

produced by geometric linear analysis were also calculated and presented in Sec. IV.C.

III. Fracture Mechanics Analysis

A. Effect of Secondary Bending on Stress Intensity Factor

Linear elastic fracture mechanics is used to calculate the principal parameters that govern fracture failure. Using the 2-D FE model and the MVCCT [7–9], the strain energy release rate (SERR or G) can be computed for the lead crack in the substrate.[§] In the absence of bending, the following equation is used:

$$G_I = -\frac{1}{2\Delta a t_s} F_s^y \Delta v_s^o = -\frac{1}{\Delta a t_s} F_s^y v_s^o \tag{4}$$

where Δa is the crack length increment, t_s is the substrate thickness, F_s^y the constraint force at the crack-tip node, and $v_s^0 = \Delta v_s^o/2$ the displacement at the node immediately behind the crack tip (see Fig. 3).

The SIF is determined by

$$K_I = \sqrt{G_I E_s^*} \tag{5}$$

where

$$E_s^* = E_s \quad \text{(plane stress)}, \qquad E_s^* = \frac{E_s}{1-\nu_s^2} \quad \text{(plane strain)} \tag{6}$$

and E_s is the elastic modulus of the plate, and ν_s the Poisson's ratio.

When bending is present, methods are available in the literature. Young and Sun [5] and Sun et al. [10] divide G into two components, one due to the traction force (G_{I_F}) and the other due to the bending moment (G_{I_M}):

$$G_{I_F} = -\frac{1}{\Delta a t_s} F_s^y v_s^o, \qquad G_{I_M} = -\frac{1}{\Delta a t_s} M_s^x \phi_s^x \tag{7}$$

where F_s^y and M_s^x are the constraint force and moment at the crack-tip node, and v_s^o and ϕ_s^x are the displacement and rotation at the first node behind the crack tip based on the Mindlin plate theory [see Eq. (2) and Fig. 3]. The SIF is also calculated in the form of two components [5,10]:

$$K_{I_F} = \sqrt{G_{I_F} E_s^*}, \qquad K_{I_M} = \sqrt{3 G_{I_M} E_s^*} \tag{8}$$

It is assumed that the SIF variation in the thickness direction is linear; thus a distribution function $K_I(z)$ is written as

$$K_I(z) = K_{I_F} + \frac{2z}{t_s} K_{I_M} \tag{9}$$

However, Wang et al. [3] and Wang and Rose [11,22] have shown that a through-thickness distribution of SIF cannot be obtained by calculating the strain energy release rate. They claim that, from an energy point of view, only the total SERR can be computed (that is $G_{I_{\text{tot}}}$) from its two components, one due to the traction (G_{I_F}) and the other one due to bending (G_{I_M}):

$$G_{I_{\text{tot}}} = G_{I_F} + G_{I_M} = -\frac{1}{\Delta a t_s}(F_s^y v_s^o + M_s^x \phi_s^x) \tag{10}$$

From this $G_{I_{\text{tot}}}$ they claim that only the rms of SIF can be calculated from Eq. (10), that is

$$K_{I_{\text{rms}}} = \sqrt{G_I E^*} = \sqrt{-\frac{1}{\Delta a t_s}(F_s^y v_s^o + M_s^x \phi_s^x) E^*} \tag{11}$$

We have developed a different approach to the aforementioned two methods. In this work, Eq. (4) is employed at different thickness levels. Based on the Mindlin plate theory, distributions of displacement and constraint force can be obtained from the nodal values as functions of the thickness variable z (see Fig. 3):

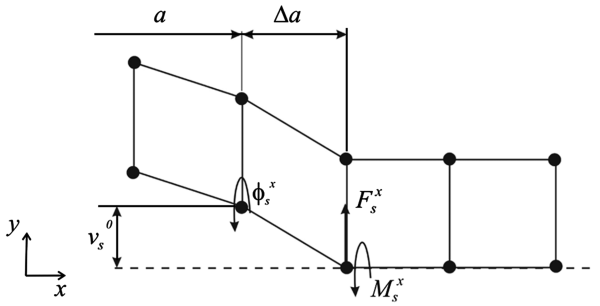

Fig. 3 Parameters used in the MVVCT for the substrate crack. The dashed line ($y = 0$) represents the symmetry of the geometry.

$$v_s(z) = v_s^0 - z\phi_s^y, \qquad F_s(z) = F_s^y - z\frac{12M_s^x}{t_s^2} \tag{12}$$

Substituting Eq. (12) in Eq. (4) the SERR distribution through the thickness can be obtained

$$\begin{aligned} G_I(z) &= -\frac{1}{\Delta a t_s} F_s(z) v_s(z) \\ &= -\frac{12M_s^x \phi_s^x}{\Delta a t_s^3} z^2 + \left(\frac{12M_s^x v_s^0}{\Delta a t_s^3} + \frac{\phi_s^x F_s^y}{\Delta a t_s}\right) z - \frac{F_s^y v_s^0}{\Delta a t_s} \end{aligned} \tag{13}$$

Using Eq. (5) to connect K_I with G_I, we obtain a K distribution:

$$K_I(z) = \sqrt{\left[-\frac{12M^0\phi}{\Delta a t^3} z^2 + \left(\frac{12M^0 v^0}{\Delta a t^3} + \frac{\phi F^0}{\Delta a t}\right) z - \frac{F^0 v^0}{\Delta a t}\right] E^*} \tag{14}$$

Thus, a through-thickness distribution of the crack front SERR and SIF can be determined. It should be noted that the mean value of the SERR [Eq. (13)] through the thickness equals the so-called "total" SERR ($G_{I_{\text{tot}}}$) derived by Wang and Rose [Eq. (10)]:

$$G_{I_{\text{mean}}} = \frac{1}{t_s}\int_{-\frac{t_s}{2}}^{\frac{t_s}{2}} G_I(z)\mathrm{d}z = -\frac{1}{\Delta a t_s}(F_s^y v_s^o + M_s^x \phi_s^x) = G_{I_{\text{tot}}} \tag{15}$$

Moreover, the rms value of the SIF obtained from Eq. (14) is analytically equal to the one found by Wang et al. [3] and Wang and Rose [11,22] [Eq. (11)], in fact,

$$K_{I_{\text{rms}}} = \sqrt{\frac{1}{t_s/2 + t_s/2}\int_{-\frac{t}{2}}^{\frac{t}{2}} K_I(z)^2 \mathrm{d}z} \tag{16}$$

Applying Eq. (5) along the thickness and Eq. (15), we get

$$\begin{aligned} K_{I_{\text{rms}}} &= \sqrt{\frac{1}{t_s}\int_{-\frac{t}{2}}^{\frac{t}{2}} G_I(z) E_s^* \mathrm{d}z} = \sqrt{G_{I_{\text{tot}}} E_s^*} \\ &= \sqrt{-\frac{1}{\Delta a t_s}(F_s^y v_s^o + M_s^x \phi_s^x) E_s^*} \end{aligned} \tag{17}$$

It can be seen that Eq. (17) is the same as Eq. (11).

The SIF obtained by this approach [Eq. (14)] is the square root of a parabola, therefore it is different analytically from the one derived by Young and Sun [5] and Sun et al. [10] [Eq. (9)]; the latter gives a linear distribution. Although the analytical expressions are different, calculated SIF values for the cases examined here are very close. This proposed method permits computing the crack front SERR and SIF along the thickness. The parabolic distribution of SERR is confirmed by a 3-D FE analysis in Sec. IV.B.

[§]In this section, SERR and SIF are for the substrate crack; hence the subscript "substrate" (s) is omitted for briefness and clarity.

B. Strain Energy Release Rate on Disbond Front and Disbond Growth Modeling

In this paper adhesive disbond growth is interactively modeled with the substrate crack propagation. In most of the literature papers on selective reinforcement or patch repairs, disbond is either not studied [3,11,13,14,22] or modeled by prescribing disbond shape and size as a function of the substrate crack length by observing the test results [6,10,12].

In this work the disbond front is determined for each substrate crack length (a). This is done by calculating the strain energy release rate for each group of the spring elements at the disbond periphery by the MVCCT method while keeping the memory of the propagation direction

$$G_{\mathrm{I}} = -\frac{F_{az}(w_{a2} - w_{a1})}{2\Delta A_a}, \qquad G_{\mathrm{II}} = -\frac{F_{ay}(v_{a2} - v_{a1})}{2\Delta A_a}$$
$$G_{\mathrm{III}} = -\frac{F_{ax}(u_{a2} - u_{a1})}{2\Delta A_a} \tag{18}$$

where F_{az}, F_{ay}, and F_{ax} are the forces in the springs, w, v, and u are the corresponding displacements of the nodes immediately behind the disbond front, and $\Delta A_a = \Delta l b_a$ is the crack extension area that is released to compute the SERR (see Fig. 4).

By using a mixed mode failure criterion [23,24] [Eq. (19)], the failing adhesive elements due to disbond growth are identified and deleted from the FE model to simulate adhesive disbond progression

$$\frac{G_{\mathrm{I}}}{G_{\mathrm{IC}}} + \frac{G_{\mathrm{II}}}{G_{\mathrm{IIC}}} + \frac{G_{\mathrm{III}}}{G_{\mathrm{IIIC}}} \geq 1 \tag{19}$$

where G_{IC}, G_{IIC}, and G_{IIIC} are the critical strain energy release rates for modes I, II, and III.[¶] If the disbond shape or size has changed, then a subsequent FE analysis is performed to find the new forces and displacements in the spring elements, recalculated the G values, and applied the failure criterion. When the disbond front is steady, that is, no more spring fails, the substrate crack-tip node is released and, by applying the MVCCT for the crack, SERR distribution is calculated for the new lead crack length. Clearly this disbond growth model does not take account of the cyclic load effect, which is the loading mode that most repaired components are subjected to. However, disbonds in the patch repair and bonded crack retarder problems are mostly due to the peak stress caused by the stress "singularity" by the substrate crack rather than fatigue cyclic loads. This disbond growth modeling technique has been validated against published experimental tests [17,19] and presented in Sec. IV.

C. Fatigue Crack Growth Calculation

The aim of this analysis method is to predict FCG life for patch repaired plates. Therefore, a material law for the FCG rate is needed. In this study the NASGRO equation [25] is chosen:

$$\frac{\mathrm{d}a}{\mathrm{d}N} = C\left[\left(\frac{1-f}{1-R}\right)\Delta K\right]^n \frac{[1 - (\Delta K_{\mathrm{th}}/\Delta K)]^p}{[1 - (K_{\max}/K_{\mathrm{crit}})]^q} \tag{20}$$

where N is the number of cycles, C, n, p, and q are material constants, f is a coefficient for the crack closure effect, ΔK_{th} is the threshold SIF, K_{crit} is the fracture toughness, $\Delta K = K_{\max} - K_{\min}$ is the applied SIF range, and $R = \sigma_{\min}/\sigma_{\max}$ is the cyclic stress ratio.

Two problems must be solved before applying this equation to compute the FCG life. The first is due to the geometric nonlinearity of the model. The second is due to the nonuniform distribution of SIF along the thickness of the crack front, but only one representative SIF value is needed for the NASGRO equation for every crack profile. The methods we have used to deal with these are presented in the following two sections.

[¶]Because of the lack of data G_{IIIC} is assumed to be equal to G_{IIC} for the adhesive used in this paper. The error is negligible because for this problem disbond is mode II dominated.

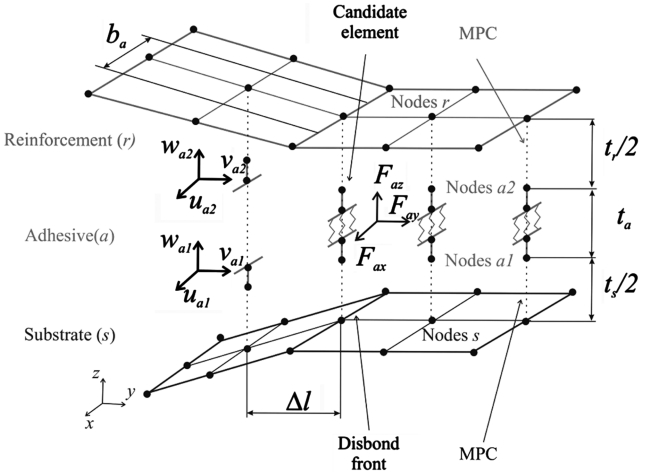

Fig. 4 Schematic of the parameters in the MVCCT for calculating the strain energy release rate for the spring elements at the disbond front.

1. *Geometric Nonlinearity: Alternate Stress Intensity Factor Analysis*

In the absence of bending, the SIF range (ΔK) of any load levels can be calculated by just one FE analysis at a given applied stress. For example, at the applied stress σ_x, K_{I_x} is calculated and a dimensionless SIF, called the geometric or β factor, can be established. This is only a function of the geometry and boundary conditions:

$$\beta = \frac{K_{I_x}}{\sigma_x \sqrt{\pi a}} \tag{21}$$

from this β factor, SIF at any given stresses, for example, maximum and minimum stresses, and the SIF range (ΔK_I) can be determined

$$K_{I_{\max}} = \beta \sigma_{\max} \sqrt{\pi a}, \qquad K_{I_{\min}} = \beta \sigma_{\min} \sqrt{\pi a}, \qquad \Delta K_I = \beta \Delta\sigma \sqrt{\pi a} \tag{22}$$

and the R ratio is

$$R = \frac{K_{I_{\min}}}{K_{I_{\max}}} = \frac{\sigma_{\min}}{\sigma_{\max}} \tag{23}$$

When the problem is geometrically nonlinear, the above relations do not hold any more, because the β factor is also a function of the applied stress,[**] that is,

$$\frac{K_{I_x}}{\sigma_x} \neq \frac{K_{I_{\max}}}{\sigma_{\max}} \neq \frac{K_{I_{\min}}}{\sigma_{\min}} \quad \text{and} \quad R = \frac{K_{I_{\min}}}{K_{I_{\max}}} \neq \frac{\sigma_{\min}}{\sigma_{\max}} \tag{24}$$

This means that the dimensionless SIF (β factor) does not exist due to the geometric nonlinearity. ΔK must be determined by running two FE analyses at the maximum and minimum applied stresses, respectively. We named this method the "alternate SIF analysis" under cyclic loads. This leads to an effective SIF range ΔK and effective R ratio, which is different from the nominal cyclic stress R ratio (see Sec. IV.C).

2. *RMS vs Weighted Stress Intensity Factor*

Another obstacle in predicting FCG rates for a crack front is the fact that SIF varies along the crack front but only one representative SIF value for each crack profile is needed for Eq. (20) to calculate FCG rates and lives. The maximum, the mean, and the rms values are all good candidates; the rms is related to the through-thickness "average total" value of the strain energy release rate. Klug et al. [12] showed that the best agreement with test results was obtained using the rms value of SIF. The maximum SIF, that is, the SIF on the unpatched side, leads to an overconservative life prediction because

[**]Displacements, stresses, and SIF are not linear with the applied stress anymore; the dependency of SIF on applied stress cannot be removed.

Table 1 Mechanical properties of substrate plate, repair patch, and adhesive found in [13,14] and used in this model

	Density	Elastic modulus			Shear modulus			Poisson's ratio		
	ρ g/cm^3	E_1 GPa	E_2 GPa	E_3 GPa	G_{12} GPa	G_{13} GPa	G_{23} GPa	ν_{12}	ν_{13}	ν_{23}
Aluminum 7075-T651 (T-L)	2.81	71.02	71.02	71.02	26.9	26.9	26.9	0.32	0.32	0.32
Carbon epoxy	1.8	134.0	10.3	10.3	5.5	5.5	3.2	0.33	0.33	0.53
Adhesive	1.1	2.76	2.76	2.76	1.04	1.04	1.04	0.32	0.32	0.32

the interactions of all other SIF values through the thickness are neglected.

To take account of the fact that the crack length at the unpatched face is dragged back by all other shorter crack lengths (and vice versa), a weight function is developed in this work. This weight function is based on the fact that the crack front, which has to be modeled as a straight line if 2-D FEs are used, actually has a parabolic shape. Assuming that the parabola vertex is at the unpatched side and the value is 1 and that the value on the patched side is 0, a parabolic equation is obtained

$$W(z) = -\frac{1}{t_s^2}z^2 - \frac{1}{t_s}z + \frac{3}{4} \tag{25}$$

Using this weight function [Eq. (25)] and the through-thickness SERR distribution [Eq. (13)], a weighted SERR (G_{I_W}) can be determined:

$$G_{I_W} = \frac{\int_{-t_s/2}^{t_s/2} W(z)G_I(z)\mathrm{d}z}{\int_{-t_s/2}^{t_s/2} W(z)\mathrm{d}z} = -\frac{9}{10}\frac{M^0\phi}{\Delta at} - \frac{1}{8}\left(\frac{12M^0v^0}{\Delta at^2} + \frac{\phi F^0}{\Delta a}\right) - \frac{F^0v^0}{\Delta at} \tag{26}$$

Similarly, a weighed SIF (K_{I_W}) can be found using Eqs. (5) and (26).

Hosseini-Toudeshky and Mohammadi [15] modeled patch repairs and compared two 3-D FE models, one having a curved crack front and the other a straight crack front (that can be modeled by 2-D FE analysis). They found that FCG life can be predicted by the simpler 3-D FE model with straight crack front using an equivalent SIF; the representative SIF is in a position along the thickness that depends on the elastic modulus of the plate and patch, as well as the plate thickness. That position was found to be between 0.32–0.37 of the plate thickness from the unpatched side. In a similar way, Eq. (26) gives a weighted SIF that can also be associated with a position on the crack front and is associated with the parabolic shape of the actual crack front.

Calculated FCG lives for three patched plates are presented in Sec. IV.D based on geometrically nonlinear analysis, that is, the alternate SIF analysis, and disbond simulation. Three different SIF values were used in the NASGRO equation for life prediction; these were the maximum (at unpatched side), the rms, and the weighted.

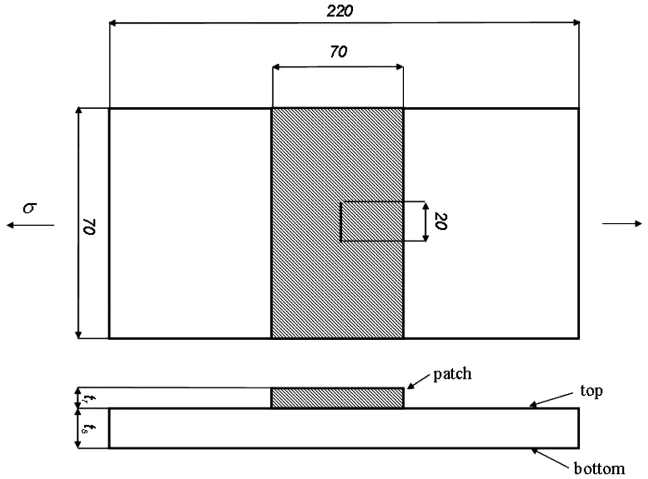

Fig. 5 Specimen configuration and geometry; initial crack length was 20 mm.

IV. Results and Discussion

A. Analysis Examples

Test results published in [13,14] are used in this study for validating the models. A test specimen is shown in Fig. 5. The substrate plate was made of aluminum alloy 7050-T651 of three different thicknesses: 2, 6, and 10 mm. The repair patch was made of unidirectional carbon/epoxy laminate with fibers in the load direction. The maximum applied stress was $\sigma_{\max} = 45$ MPa at a stress ratio of $R = 0.1$. The patch thickness also varied in order to have a constant stiffness ratio defined as [13,14]

$$S = \frac{E_r t_r}{E_p t_s} = 1 \tag{27}$$

where E_p and E_r, and t_s and t_r are, respectively, the Young's modulus and thickness of the plate and reinforcement patch. Mechanical properties for the substrate plate, patch, and adhesive are given in Table 1.

B. Effect of Secondary Bending

This section presents calculated SERR and SIF distributions through the thickness and validation by a 3-D FE model (also performed by the authors). The specimen was 6 mm thick and the geometry is shown in Fig. 5. Disbond was not modeled at this stage in order to focus on the influence of secondary bending on SERR and SIF distributions.

In Fig. 6 the SERR distribution through the thickness is shown for four crack lengths. It can be seen that the difference between the 2-D (G_I 2-D) and 3-D (G_I 3-D) results is relatively small. It should be noted that a parabolic fitting curve (G_I 3-D par) perfectly fits the shape of the SERR obtained by the 3-D model with an exception at the bottom and top of the plate.[††] This confirms that the SERR distribution has a parabolic shape. In Fig. 7 the corresponding SIF distributions along the crack front are shown. It can be seen that the difference between 2-D (K_I 2-D) and 3-D (K_I 3-D) FE results is small. The SIF computed by the 2-D FE analysis looks like a line but it is actually the square root of a parabola [Eq. (14)]. For the 3-D FE results a fitting line (K_I 3-D lin) was plotted and the difference in shape is small but noticeable. In Fig. 8 both SERR and SIF obtained by 2-D and 3-D FE analysis are plotted against the crack length for different positions through the thickness. Good agreement is achieved between the 2-D and 3-D FE analysis results, thus the 2-D modeling technique developed in this work is suitable to compute the secondary bending effect and the SERR and SIF distributions through the thickness.

C. Effect of Geometric Nonlinearity

The geometric nonlinearity effect was studied for the 2 mm thick substrate of the same dimension described in Fig. 5. Thinner substrates demonstrate a more distinct effect of geometric nonlinearity. Disbond was not considered for this analysis. In the following discussion, linear analysis refers to geometrically liner FE

[††]The degree of crack-tip stress singularity where a crack front intersects with a free surfaces differs from the inverse-square-root singularity developed for the usual crack problem; consequently at free surfaces cracks cannot be characterized by the SIF [26].

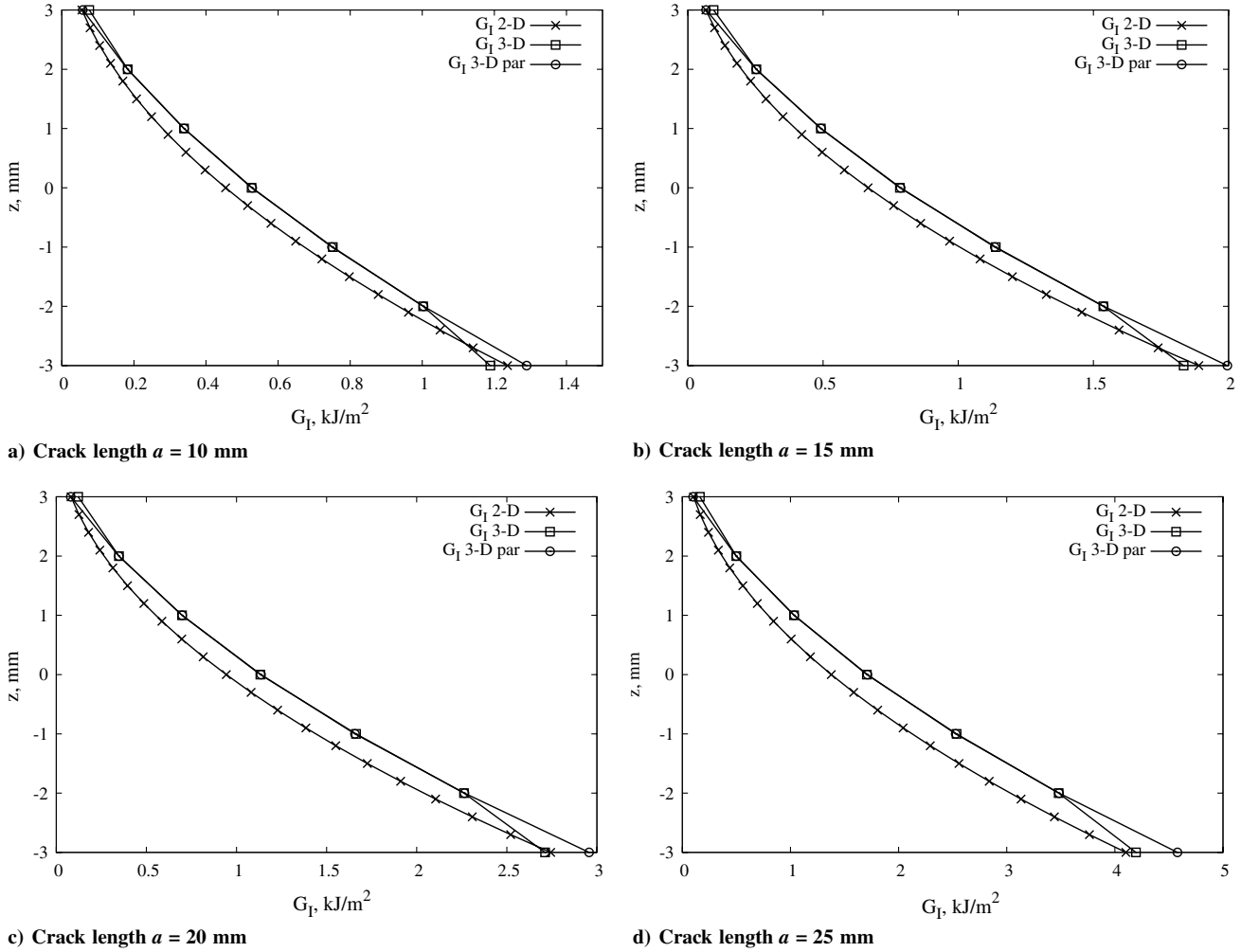

a) Crack length a = 10 mm

b) Crack length a = 15 mm

c) Crack length a = 20 mm

d) Crack length a = 25 mm

Fig. 6 SERR (G_I) distributions along the thickness for different crack lengths: comparison of 2-D and 3-D FE models, and also with a parabolic fitting of the 3-D results (noted as "3-D par"); 6-mm-thick aluminum plate with repair patch; $z = 3$ mm represents the patched side.

analysis; the β factor is calculated from an SIF value. Any other SIF values at different applied stresses can then be determined by the β factor [Eqs. (21) and (22)]. Nonlinear analysis refers to a geometrically nonlinear FE analysis; load is applied step by step on a deformed configuration caused by previous load steps. As shown in Sec. III.C.1, two analyses are required to compute the effective SIF range because the secondary bending effect will affect SIF, which can no longer be scaled by the β factor.

Figure 9a shows the difference in SIF by the linear (L) and nonlinear (NL) analyses. In Fig. 9b the SIF range computed by linear analysis is compared with that calculated by the "alternate analysis" method, marked as NL (see Sec. III.C.1). It can be seen that geometrically nonlinear analysis is necessary; otherwise over-conservative FCG life will be predicted.

In Fig. 10a the SIF range computed by a single nonlinear analysis at the maximum applied stress [$\Delta K_I = K_{I_{\max}}(1 - R)$] is compared with the true SIF range computed by the alternate SIF method (ΔK_I eff). The nonlinearity also produces an effective R ratio (R eff) that is different from the applied cyclic stress ratio (stress R) (see Fig. 10b). Thus, to compute the effective SIF range and R ratio by nonlinear analysis, a single FE analysis is not enough; the alternate SIF method must be employed (Fig. 10).

D. Fatigue Crack Growth Life Prediction

FCG life was computed for the 2, 6, and 10 mm thick substrates. The FE modeling has covered the effects of secondary bending, disbond failure, and geometric nonlinearity. Test results used here were obtained by Lee and Lee [13,14]. In [13,14] 3-D numerical models were also developed and the lives were computed using the Paris equation. It is noted that different Paris coefficients for different plate thicknesses were used, even though they are supposed to be material constants. In this study the NASGRO equation and its material database [27] were used. The material coefficients were the same for any plate thickness. The calculated SIF range and effective R ratio as a function of the crack length were input in the NASGRO equation to compute the FCG life. In Fig. 11 FCG lives obtained by using the unpatched side, the root mean square, or the weighted values of SIF ranges are plotted and compared with the test results. It can be seen that the best agreement with the test results is obtained by using the weighted SIF solution. The final FCG lives and the errors obtained from the models are shown in Table 2.

Given the scatter that is associated with the fatigue crack propagation tests, the modeling technique and the fracture mechanics calculations introduced in Secs. II and III are considered to be validated.

E. Parametric Study

Having validated the modeling technique against experiments, a parametric study of the effect of the stiffness ratio [Eq. (27)] on the FCG life is carried out. A project graph is developed to compare different patch geometries and to help in selecting the lightest one to achieve a life target (Sec. IV.E.2).

1. Effect of Stiffness Ratio

The influence of the stiffness ratio [Eq. (27)] was studied for two substrate thicknesses (2 and 6 mm). In Fig. 12 the so-called "life improvement factor," that is the FCG life of patch reinforced plates

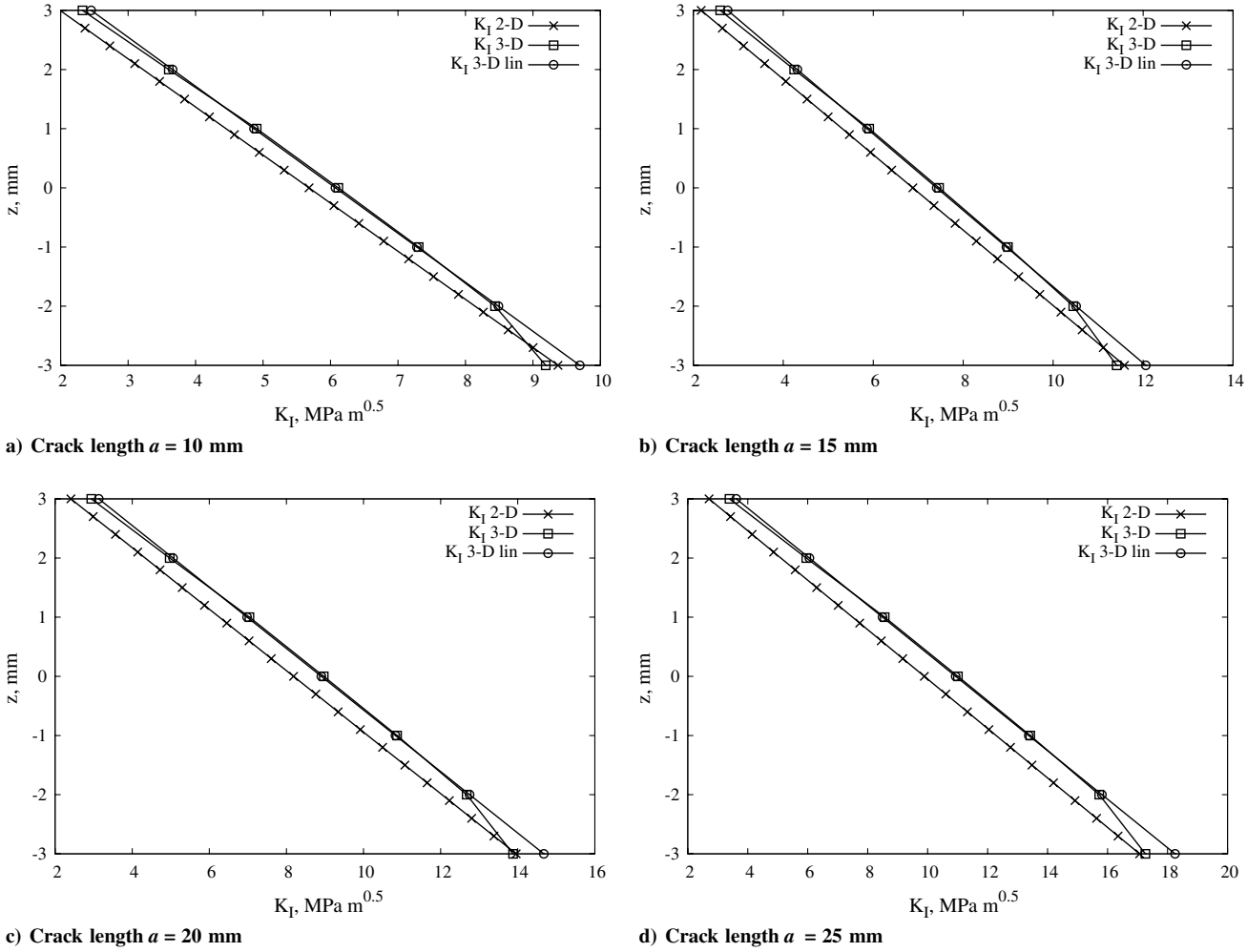

a) Crack length a = 10 mm **b) Crack length a = 15 mm**

c) Crack length a = 20 mm **d) Crack length a = 25 mm**

Fig. 7 SIF (K_I) distributions along the thickness for different crack lengths: comparison of 2-D and 3-D FE models, and also with a linear fitting of the 3-D results (noted as "3-D lin"); 6-mm-thick aluminum plate with repair patch; z = 3 mm represents the patched side.

normalized by that of unreinforced, is plotted against the stiffness ratio (S). It can be seen that the higher the ratio, the longer the life. It is also worth noting that under the same stiffness ratio more life improvement could be achieved for a thinner substrate. It means that the patch repair technique is more effective for thin substrates. To improve the FCG life in a thick substrate, a thicker patch is required.

2. Project Graph

From Fig. 12, the higher the stiffness ratio, the more life improvement. Unfortunately, this also means that the repair patch would be larger or thicker, increasing the structural weight and cost. To achieve a prescribed FCG life by using the most effective patch geometry, a project graph should be used. It is a graph that can lead

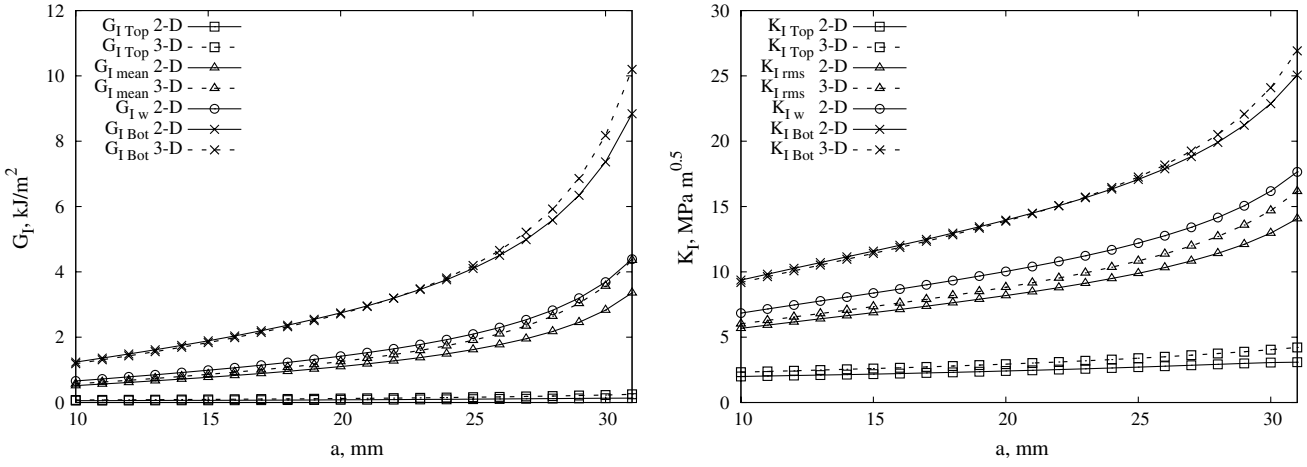

a) SERR G_I versus crack length **b) SIF K_I versus crack length**

Fig. 8 Comparison between 2-D and 3-D FE analysis of SERR (G_I) and SIF (K_I) versus crack length in different thickness positions. Top and Bot indicate the patched and unpatched sides, respectively; the mean value of SERR is linked to the rms of SIF, and w is the weighted value.

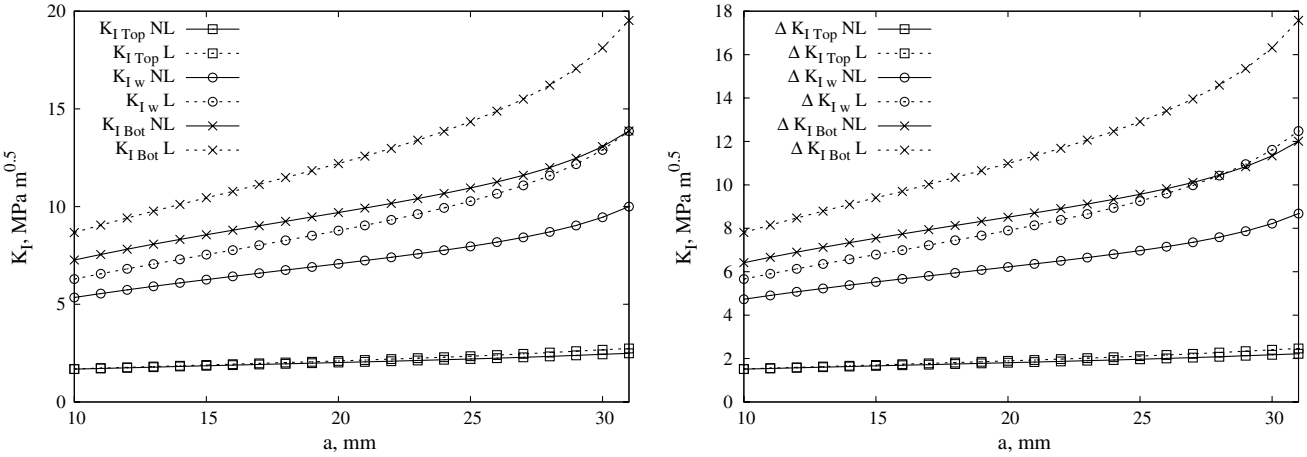

a) K_I versus crack length **b) ΔK_I versus crack length**

Fig. 9 Comparison between linear (L) and geometrically nonlinear (NL) analyses for the 2-mm-thick plate with a repair patch. Parameters are plotted for different positions along the thickness: Top and Bot indicate the patched and unpatched sides, respectively, and w is the weighted solution.

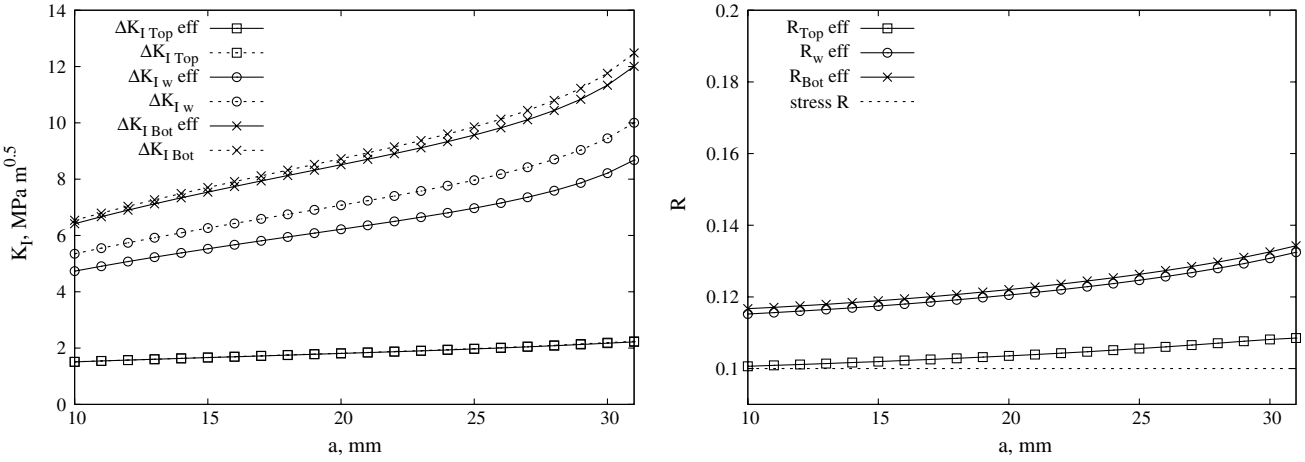

a) ΔK_I versus crack length **b) R ratio versus crack length**

Fig. 10 Comparison between two geometrically nonlinear analyses for the 2-mm-thick substrate plate in terms of SIF range and R ratio. One solution was determined by just one nonlinear analysis at the maximum stress, and the other used the "alternate analysis" (effective values). Each parameter represents a position through the plate thickness: Top and Bot indicate patched and unpatched sides, respectively, and w is the weighted value.

the designer to the best patch geometry for a given fatigue life target (see Fig. 13). It was originally developed by the authors in [17].

The x axis shows the width ratio (w_r/w_s = repair patch width/substrate width). The left y axis is the percentage life increment ΔN [Eq. (28)] and the right y axis shows the percentage of structural mass increment Δm [Eq. (29)] due to the patch

$$\Delta N = \frac{N_{\text{reinf}} - N_{\text{unreinf}}}{N_{\text{unreinf}}} \times 100 \tag{28}$$

$$\Delta m = \frac{(m_r + m_s) - m_s}{m_s} \times 100 = \frac{m_r}{m_s} \times 100 \tag{29}$$

where N_{reinf} and N_{unreinf} are the FCG lives of the reinforced and unreinforced substrates, respectively, and m_r and m_s are the weights of the repair patch and substrate, respectively.

In the graph there are three pairs of curves. Each pair refers to a specific thickness ratio (t_r/t_s = repair patch thickness/substrate thickness), or a stiffness ratio (S), and is indicated by a unique symbol (triangle, square, or circle). For each pair of curves, the solid line refers to the life increment and is read on the left axis, and the dashed line refers to the mass increment and is read on the right axis. As an example, two project graphs for two substrate thicknesses (2 and 6 mm) are shown in Fig. 13.

Table 2 Comparison of predicted and measured FCG lives and errors

t_s, mm	2		6		10	
Test FCG life [13]	250,000	325,000	90,000	98,000	68,000	76,000
RMS	403,800		147,800		104,300	
	+61.52%	+24.24%	+64.22%	+50.81%	+53.38%	+37.24%
Weighted	295,400		108,100		75,100	
	+18.16%	−9.11%	+20.11%	+10.3%	+10.44%	−6.44%
Unpatched side	136,100		47,600		30,700	
	−45.56%	−66.43%	−47.11%	−51.43%	−54.85%	−59.61%

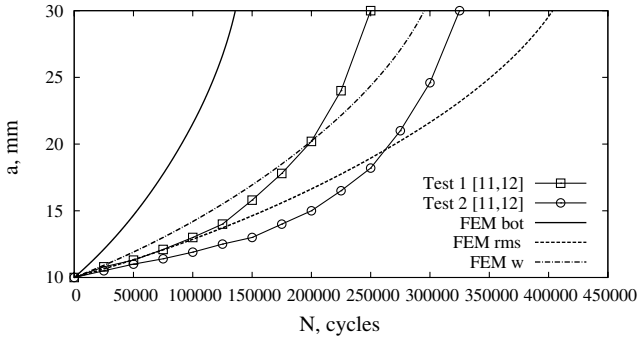

a) 2-mm-thick plate

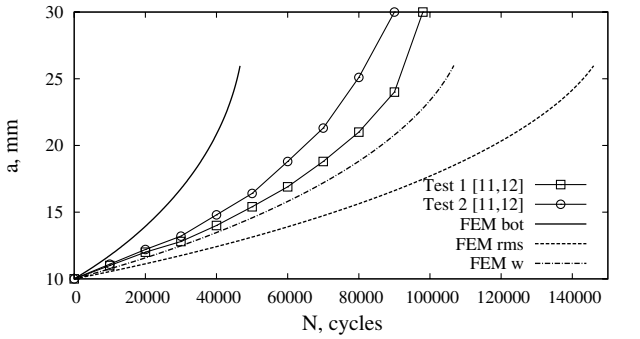

b) 6-mm-thick plate

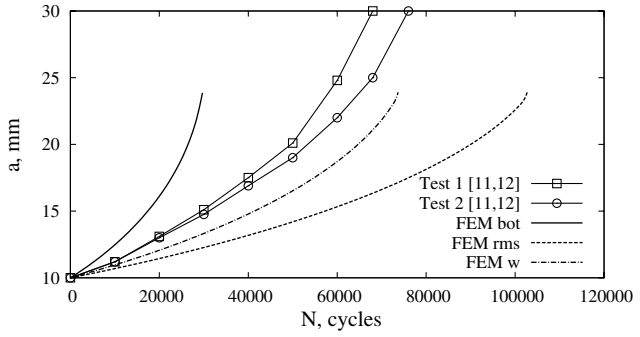

c) 10-mm-thick plate

Fig. 11 Computed FCG lives against test results from [13,14] for three different substrate thicknesses. The predicted FCG life was computed by three representative SIF range values through the thickness: Bot indicates the unpatched side, rms the root means square, and w the weighted value.

Figure 13a is explained to show how to use the project graph. First, a life increment target is decided, for instance, 3 times or 300% life increment. Following the horizontal arrow three strap geometries that are able to produce that specified life increment target can be found. The weight increment that corresponds to those three solutions can be read on the right axis; consequently, the lightest patch geometry able to achieve that life target can be found. In this case the weight increment is just under 3% for $S = 0.5$.

Another example for a thicker substrate (6 mm) is shown in Fig. 13b. After deciding a life improvement target, for example, 175%, the lightest patch able to reach it can be found. To summarize, if a project graph is established, the lightest and most effective patch geometry can be found for a given life improvement target.

V. Conclusions

The relevant failure mechanisms affecting patch repaired plates have been assessed by means of an enhanced 2-D FE modeling technique that takes into account the substrate crack propagation as well as the disbond failure of the adhesive bond. Equations to compute the SERR and the SIF along the crack front have been developed to take into account the secondary bending effect. This 2-D method is validated against a 3-D FE model.

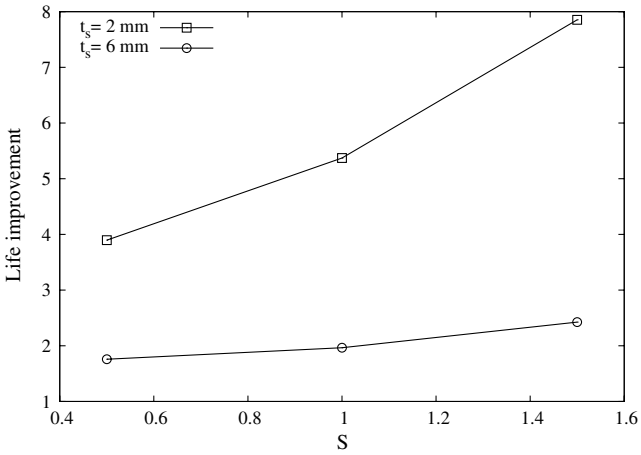

Fig. 12 FCG life improvement as a function of the stiffness ratio for two substrate thicknesses: 2 and 6 mm.

The effect of geometric nonlinearity inherent of the single-sided patched plates has been shown in terms of the SIF, SIF range, and effective R ratio, and a methodology called alternate SIF analysis has been employed to compute the effective SIF range and R ratio. To deal with the effect of crack front curvature, a weight function has been developed to take into account the interactions of the different

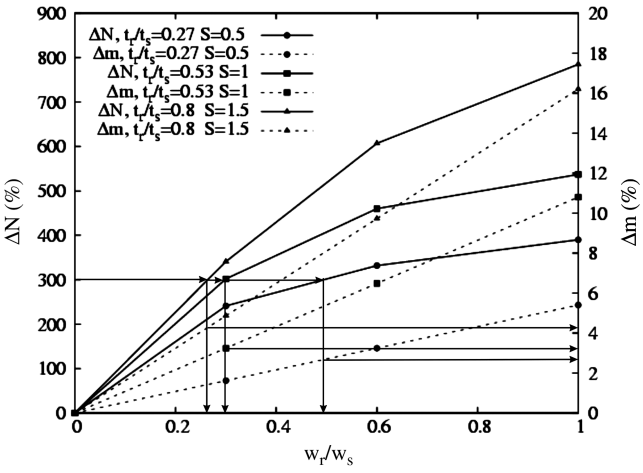

a) 2-mm-thick substrate

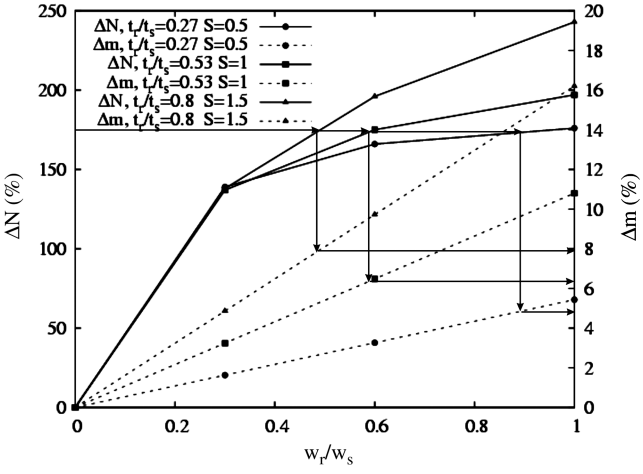

b) 6-mm-thick substrate

Fig. 13 Project graph: examples and demonstration of its application.

SIF values through the thickness and crack front shape; the FCG lives were computed by integrating the SIF values of the unpatched side, rms, and weighted average, and the best agreement with the test results was obtained by the weighted SIF value.

The effect of the patch/substrate stiffness ratio was also studied. The higher the stiffness ratio, the better the FCG life improvement. Unfortunately, a higher stiffness ratio requires either a stiffer patch material or a thicker patch; the latter means increased structural weight. To find the most effective patch geometry, the project graph was developed. By using this tool, once a life improvement target is decided, all the patch geometries able to reach that life target can be found with their corresponding weight gains. The lightest solution can be found for a given life.

Finally, it is worth noticing that the bonded patch repair technique is much more effective on thin substrates, that is, the same stiffness ratio produces a larger life increment for a thinner substrate than it does for a thicker substrate.

Acknowledgments

The authors are grateful to Airbus and Alcoa, Inc., for providing financial support.

References

[1] Baker, A. A., Rose, L. R. F., and Jones, R., *Advanced in the Bonded Composite Repair of Metallic Aircraft Structure*, Elsevier, New York, 2002.

[2] Baker, A. A., "Fibre Composite Repair of Cracked Metallic Aircraft Components-Pratical and Basic Aspects," *Composites*, Vol. 18, No. 4, 1987, pp. 293–308. doi:10.1016/0010-4361(87)90293-X

[3] Wang, C. H., Rose, L. R. F., and Callinan, R., "Analysis of Out-of-Plane Bending in One-Sided Bonded Repair," *International Journal of Solids and Structures*, Vol. 35, No. 14, 1998, pp. 1653–1675. doi:10.1016/S0020-7683(97)00129-7

[4] Rose, L. R. F., "A Cracked Plate Repaired by Bonded Reinforcements," *International Journal of Fracture*, Vol. 18, No. 2, 1982, pp. 135–144. doi:10.1007/BF00019638

[5] Young, M. J,. and Sun, C. T., "On the Strain Energy Release Rate for Cracked Plate Subjected to Out-of-Plane Bending Moment," *International Journal of Fracture*, Vol. 60, No. 3, 1993, pp. 227–247. doi:10.1007/BF00012511

[6] Arendt, C., and Sun, C. T., "Bending Effects of Unsymmetric Adhesively Bonded Composite Repairs on Cracked Aluminum Panels," *Proceedings of the FAA/NASSA Symposium on Advanced Integrity Methods for Airframe Durability and Damage Tolerance, Pt. 1*, 1994, pp. 33–48.

[7] Rybicki, E., and Kanninen, M., "A Finite Element Calculation of Stress Intensity Factors by a Modified Crack Closure Integral," *Engineering Fracture Mechanics*, Vol. 9, No. 4, 1977, pp. 931–938. doi:10.1016/0013-7944(77)90013-3

[8] Raju, I., "Calculation of Strain Energy Release Rate with Higher Order and Singular Finite Elements," *Engineering Fracture Mechanics*, Vol. 28, No. 3, 1987, pp. 251–274. doi:10.1016/0013-7944(87)90220-7

[9] Krueger, R., "The Virtual Crack Closure Technique: History, Approach and Applications," ICASE, ICASE Mail Stop 132C, NASA Langley Research Center, Rept. No. 2002-10 NASA/CR-2002-211628, 2002.

[10] Sun, C. T., Klug, J., and Arendt, C., "Analysis of Cracked Aluminium Plates Repaired with Bonded Composite Patches," *AIAA Journal*, Vol. 34, No. 2, 1996, pp. 369–374. doi:10.2514/3.13073

[11] Wang, C. H., and Rose, L. R. F., "A Crack Bridging Model for Bonded Plates Subjected to Tension and Bending," *International Journal of Solids and Structures*, Vol. 36, No. 13, 1999, pp. 1985–2014. doi:10.1016/S0020-7683(98)00070-5

[12] Klug, J., Maley, S., and Sun, C. T., "Characterization of Fatigue Behavior of Bonded Composite Repairs," *Journal of Aircraft*, Vol. 36, No. 6, 1999, pp. 1016–1022. doi:10.2514/2.2543

[13] Lee, W.-Y., and Lee, J.-J., "Fatigue Behavior of Composite Patch Repaired Aluminum Plate," *Journal of Composite Materials*, Vol. 39, No. 16, 2005, pp. 1449–1463. doi:10.1177/0021998305050435

[14] Lee, W.-Y., and Lee, J.-J., "Successive 3D FE Analysis Technique for Characterization of Fatigue Crack Growth Behavior in Composite-Repaired Aluminum Plate," *Composite Structures*, Vol. 66, Nos. 1–4, 2004, pp. 513–520. doi:10.1016/j.compstruct.2004.04.074

[15] Hosseini-Toudeshky, H., and Mohammadi, B., "A Simple Method to Calculate the Crack Growth Life of Adhesively Repaired Aluminum Panels," *Composite Structures*, Vol. 79, No. 2, 2007, pp. 234–241. doi:10.1016/j.compstruct.2006.01.005

[16] Hosseini-Toudeshky, H., Mohammadi, B., Sadeghi, G., and Daghyani, H. R., "Numerical and Experimental Fatigue Crack Growth Analysis in Mode-I for Repaired Aluminum Panels Using Composite Material," *Composites Part A: Applied Science and Manufacturing*, Vol. 38, No. 4, 2007, pp. 1141–1148. doi:10.1016/j.compositesa.2006.06.003

[17] Boscolo, M., Allegri, G., and Zhang, X., "Design and Modelling of Selective Reinforcements for Integral Aircraft Structures," *AIAA Journal*, Vol. 46, No. 9, 2008, pp. 2323–2331. doi:10.2514/1.35712

[18] Zhang, X., Figueroa-Gordon, D., Boscolo, M., Allegri, G., and Irving, P. E., "Improving Fail-Safety of Aircraft Integral Structures Through the Use of Bonded Crack Retarders," *Proceedings of the 24th Symposium of International Committee on Aeronautical Fatigue, ICAF 2007*, PACINIeditore, May 2007.

[19] Zhang, X., Boscolo, M., Figueroa-Gordon, D., Allegri, G., and Irving, P. E., "Fail-Safe Design of Integral Metallic Aircraft Structures Reinforced by Bonded Crack Retarders," *Engineering Fracture Mechanics*, Vol. 76, No. 1, 2009, pp. 114–133. doi:10.1016/j.engfracmech.2008.02.003

[20] Tahmasebi, F., "Software Tools for Analysis of Bonded Joints," NASA/GSFC, TR 542, 2001.

[21] Mindlin, R., "Influence of Rotatory Inertia and Shear on Flexural Motions of Isotropic Elastic Plates," *Transactions of the American Society of Mechanical Engineers, Journal of Applied Mechanics*, Vol. 18, 1951, pp. 31–38.

[22] Wang, C. H., and Rose, L. R. F., "On the Design of Bonded Patches for One-Sided Repair," *Proceedings of the 11th International Conference on Composite Materials*, July 1997, pp. 347–356.

[23] Camanho, P. P., and Dàvila, C., "Mixed-Mode Decohesion Finite Elements for the Simulation of Delamination in Composite Materials," NASA TR TM-2002-211737, June 2002.

[24] Kutlu, Z., and Chang, F., "Modeling Compression Failure of Laminated Composites Contain Multiple Through-the-Width Delaminations," *Composite Materials*, Vol. 26, No. 3, 1992, pp. 350–387. doi:10.1177/002199839202600303

[25] Forman, R., and Mettu, S., "Behavior of Surface and Corner Cracks Subjected to Tensile and Bending Loads in Ti-6Al-4V Alloy," *Fracture Mechanics 22nd Symposium*, ASTM STP 1131, ASTM, Philadelphia, PA, 1992.

[26] Lin, X. B., and Smith, R. A., "Finite Element Modelling of Fatigue Crack Growth of Surface Cracked Plates. Part 1: The Numerical Technique," *Engineering Fracture Mechanics*, Vol. 63, No. 5, 1999, pp. 503–522. doi:10.1016/S0013-7944(99)00040-5

[27] Harter, J., *AFGROW Users Guide and Technical Manual*, Air Vehicles Directorate, afrl-va-wp-tr-2006-xxxx ed., June 2006.

A. Palazotto
Associate Editor